

**Title:**

Influence of Surface Roughness on the Lubrication Effect of Carbon Nanoparticle-Coated Steel Surfaces

**Authors:**

Leander Reinert, Silas Schütz, Sebastian Suarez, Frank Mücklich

This is a post-peer-review, pre-copyedit version of an article published in *Tribology Letters*

The final authenticated version is available online at: <https://doi.org/10.1007/s11249-018-1001-6>

**Cite as:**

Reinert, L., Schütz, S., Suárez, S. et al. Tribol Lett (2018) 66: 45. <https://doi.org/10.1007/s11249-018-1001-6>



# Influence of surface roughness on the lubrication effect of carbon nanoparticle-coated steel surfaces

*L. Reinert\**, *S. Schütz*, *S. Suárez*, and *F. Mücklich*

Department of Materials Science, Saarland University, Campus D3.3, D-66123, Saarbrücken, Germany

\* *Corresponding author. Tel/Fax: +49 (681) 302 70544/70502. E-mail address: l.reinert@mx.uni-saarland.de (L. Reinert)*

## Acknowledgements

The present work is supported by funding from the Deutsche Forschungsgemeinschaft (DFG, project: MU 959/38-1 and SU 911/1-1). L. R., S.S., and F. M. wish to acknowledge the EFRE Funds of the European Commission for support of activities within the AMELab project. This work was supported by the CREATE-Network Project, Horizon 2020 of the European Commission (RISE Project No. 644013).

## Keywords

Solid lubrication; Carbon nanotubes; Onion-like carbon; lubrication mechanisms; Surface roughness

## Abstract

In the present study, a systematic evaluation of the influence of the surface roughness on the lubrication activity of multiwall carbon nanotubes (MWCNT) and onion-like carbon (OLC) is performed. MWCNT and OLC are chosen as they both present an  $sp^2$ -hybridization of carbon atoms, show a similar layered atomic structure and exhibit the potential to roll on top of a surface. However, their morphology (size and aspect ratio) clearly differs, allowing for a methodical study of these differences on the lubrication effect on systematically varied surface roughness. Stainless steel platelets with different surface finishing were produced and coated by electrophoretic deposition with OLC or MWCNT. The frictional behavior is recorded using a ball-on-disc tribometer and the resulting wear tracks are analyzed by scanning electron microscopy in order to reveal the acting tribological mechanisms. It is found, that the lubrication mechanism of both types of particles is traced back to a mixture between a rolling motion on the surfaces and particle degradation, including the formation of nanocrystalline graphitic layers. This investigation further highlights, that choosing the suitable surface finish for a tribological application is crucial for achieving beneficial tribological effects of carbon nanoparticle lubricated surfaces.

## 1 Introduction

The tribological optimization of various technical systems is dictated by the demand for lower energy consumption and in most cases, is directly linked to an efficient lubrication [1]. Certainly, the most established way to reduce friction and wear lies in the use of a suitable fluid lubrication medium. However, certain mechanical systems set the need to replace fluid with solid lubricants, as when the system runs under unfavorable environmental conditions such as high temperatures or vacuum [2, 3].

In this regard, along with classical solid lubricants (e.g. graphite or  $MoS_2$ ), carbon nanomaterials have shown to be very promising candidates for these applications [4–7]. This fact is traced back to their intrinsic physical properties, morphology and low density compared to other materials [8–10]. The focus of this work is on multi-wall carbon nanotubes (MWCNT) [11] and onion-like carbons (OLC) [12]. MWCNT can be described

as multi-shell graphitic cylinders with large aspect ratio [11]. OLC show a similar multi-shell graphitic carbon structure. However, as OLC are fullerene-like nanoparticles with a polyhedral form and a typical diameter of only 4-10 nm, they are often ascribed to be “zero dimensional” [12, 13].

In case of MWCNTs, several works confirm their ability to reduce friction and wear when used as protective films [5, 6, 14, 15], solid lubricant [16–18], reinforcement phase in composites [19–21] or lubricant additive [22–24]. Some studies are based on the assumption that CNTs form a carbonaceous layer on the surface, which presents similar tribomechanisms to those of graphite [15, 21]. Others explain these beneficial effects with their ability to efficiently separate the sliding surfaces while acting as roller bearings [7, 16, 25]. In this regard and depending on the applied contact pressure, a so called “tank-belt” effect has already been simulated and reported in literature, describing the deformation of rolling CNT between two contacting surfaces under shear [26, 27]. The deformation of the CNT and rolling movement could lead to delamination and the formation of flake-like graphitic structures. Further on, the possibility to reduce surface oxidation and thus hindering the formation of abrasive third bodies in the tribological contact might also influence the observed tribological behavior [7, 14].

Considering the polyhedral form, low amount of dangling bonds on their surface and also their potentially high mechanical strength, it is reasonable to assume that OLC might act as ball bearings in a tribological contact as well [8]. In the case of an nominally perfectly flat surface (silicon wafer), OLC coating showed a friction coefficient lower than 0.05 and also a wear reduction by 3 to 6 orders of magnitude compared to a graphite lubrication [28]. In this respect, with the curvature of OLCs being higher compared to MWCNTs, it is supposed that they show less intermolecular interactions to the surface and thus are able to freely move [29, 30]. This lubrication effect can also be maintained under vacuum conditions [28]. Despite these very promising statements of OLC as solid lubricant, there is a significant drawback. OLC lubrication decreases significantly when the normal contact pressure exceeds a certain threshold value [31]. It is also assumed that, depending on the OLC particle size, they might be trapped within the asperities of a given surface roughness and therefore no longer provide a lubricating effect [28]. However, this being a very important point, there is no systematic study comparing the effect of the surface roughness on the lubrication activity of CNP for the same tribological system yet.

Considering the surface roughness, it often defines the characteristic of a tribological system [32–35]. However, it is often linked to the final application, as this determines how much effort can be put in the design or processing of a surface. For example, surface roughness is rather low and well defined in microelectromechanical systems (MEMS) [36], whereas it is usually high in the case of large technical surfaces of machine elements [35]. With the initial work of Bowden and Tabor, the interaction between asperities of a rough surface with regard to the influence on the frictional behavior became a much discussed topic [37]. This interaction could be correlated to adhesion/welding and subsequent releasing (in case that a critical shear stress is applied), and depends upon several factors such as the electronic structure of the materials, free surface energies, interlayers and ambient conditions [33, 38]. The friction behaviors of rough surfaces are further influenced by plastic deformation and consequently, on deformation energies, contact angles between asperities or the mechanical properties of the contacting materials [38]. Concerning these interactions, it was shown that very small shear stresses are possible between atomically flat surfaces with non-matching surface corrugations, allowing for vanishing friction [39, 40]. Several different models tried to explain the interaction of two contacting surfaces under dry conditions and different scales, starting at molecular level, like for example the

Tomlinson or the Frenkel-Kontorova model [41, 42]. Based on the effects of macroscopic surface roughness on friction, numerous works successfully manipulated the stochastic surface roughness so as to create specifically designed surface geometries in order to control the coefficient of friction [14, 43–47]. Generally, adjusting a specific roughness for a given tribological application can be crucial, as it majorly determines contact mechanics and thus if a contact situation is elastic or elasto-plastic and if a real contact area is large or small [33]. Accordingly, different contact simulation models rely on surface descriptive parameters, as for example the Greenwood-Williamson, Jackson-Green or the Persson model [48–50].

However, when it comes to the use of nanoparticles as lubricants, surface roughness also plays an important role [27, 51, 52]. There are many studies about different kinds of nanoparticles (for example MWCNT, MoS<sub>2</sub>, nanodiamonds, OLC, alumina, amongst others) used as lubricant additives [22, 30, 53–58]. Most of them refer to the shape, nanostructure, surface functionalization, concentration or the size of the particles being the most important characteristics for an efficient lubrication. Considering nanoparticles as solid lubricant and not as lubricant additive, their shape and size compared to the surface roughness become even more important, as particles can be trapped, entirely be removed from the direct tribological contact or hindered in their rolling movement by surface asperities [14, 28]. Nonetheless, simulations or experiments regarding the solid lubrication activity of inorganic or organic nanoparticles so far concentrate on very low roughness surfaces like for example Si-wafer [31, 59].

Thus, the present study is motivated by the need to classify the lubrication effect of carbon nanoparticles (CNP) as solid lubricant for different surface roughness's. This could be beneficial as a steppingstone for further research, as the size and morphology of CNPs could be selected in order to fit the tribological requirements.

For this purpose, a suitable technique must be found in order to coat surfaces with a pre-defined surface roughness in a reproducible and controllable way. There are different techniques available for carbon nanoparticle coating of metallic surfaces, including spray [60] and dip coating [61], CVD [62], drop casting [7], etc. One of the most suitable and straightforward techniques is electrophoretic deposition (EPD) [63]. In contrast to drop casting or spray coating, EPD provides the advantage of being easily scalable, very homogeneous and reproducible [14, 63, 64]. Therefore, it is used in the present study.

Concerning the CNP coatings, MWCNT and OLC are chosen since they present similar atomic arrangement as well as possible lubrication mechanism (rolling mechanism). Their different morphology and particle size allow for a systematic investigation of the lubrication activity as a function of the initial surface roughness of a defined tribological system. Thus, stainless steel surfaces with different pre-defined surface roughness are coated with OLC or MWCNT, respectively. Stainless steel is used as substrate material because of its technological relevance.

## **2 Experimental Section**

### 2.1 Materials

Austenitic stainless steel (AISI 316L) platelets (20x20x1 mm<sup>3</sup>) are used as substrate material for the tribological experiments. For the coatings, MWCNTs were purchased at graphene supermarket (diameter 20-85 nm, length 5-15 μm) and OLC were synthesized from detonation nanodiamond powder (purchased from NaBond Technologies Co., purity > 98%, individual particle diameter 4–8 nm). This is done by annealing at 1750°C for 3 h in graphite crucibles in a vacuum furnace with tungsten heaters (model: 1100-3580-W1, Thermal

Technology Inc.) applying a heating and cooling rate of  $15\text{ }^{\circ}\text{C min}^{-1}$ . The chamber pressure is between 10 mPa and 100 mPa. The synthesized OLC show an individual particle diameter of 4-10 nm and almost full  $\text{sp}^2$  carbon hybridization as can be seen in prior studies [13, 65].

### 2.2 Surface preparation and characterization

The stainless steel platelets are ground flat using a fully automated grinding and polishing device (TegraPol by Struers). The surfaces were then polished up to different end-finishes. Two samples are polished using 2500 grit sandpaper from Leco corp. (MI, USA), which corresponds to a  $(8.5 \pm 0.5)\text{ }\mu\text{m}$  particle size. Furthermore, two samples of each kind are polished using  $6\text{ }\mu\text{m}$ ,  $3\text{ }\mu\text{m}$  and  $1\text{ }\mu\text{m}$  diamond polishing suspensions, respectively. Finally, also two samples are polished using a  $0.5\text{ }\mu\text{m}$  oxide polishing suspension (OPS) to achieve the lowest surface roughness. In the following, the samples are designated as  $8.5\text{ }\mu\text{m}$ ,  $6\text{ }\mu\text{m}$ ,  $3\text{ }\mu\text{m}$ ,  $1\text{ }\mu\text{m}$  and  $0.5\text{ }\mu\text{m}$ , respectively. Subsequently, these surfaces are characterized in terms of their resulting surface roughness (root mean squared roughness,  $R_{\text{rms}}$ ) using a white light interferometer (WLI, Zygo NewView 7300) equipped with a 3-D imaging surface structure analyzer. The micrographs were recorded using a 50x objective and providing a surface height resolution of  $< 0.1\text{ nm}$ . Each sample is measured 10 times at different spots from which the mean value and standard deviation is determined. Additionally, SEM micrographs of each surface were acquired using a FIB/FE-SEM dual beam station (FEI Helios Nanolab) using an acceleration voltage of 5 kV and a current of 1.4 nA.

### 2.3 EPD process

For the deposition process, the as-prepared platelets were thoroughly cleaned in order to remove possible contaminants. This was carried out by 10 min of ultrasonication (Sonorex Super RK 514 BH by Bandelin, 860 W, 35 kHz) respectively in cyclohexane, followed by acetone and finally isopropanol. Afterwards, the platelets are used as electrodes. A dispersion with a concentration of  $0.25\text{ mg}\cdot\text{ml}^{-1}$  CNT or OLC was prepared using acetone as solvent. In order to disperse the particles, a shear mixer (Ultra-turrax T-25 by IKA) was used for 5 min followed by ultrasonic treatment of the dispersion for another 20 min [65]. Subsequently, triethylamine (TEA) was added in order to add negatively charged  $\text{COO}^-$  surface groups [66]. Finally, the negatively charged CNPs are deposited in a deposition cell at a voltage of 20 V for 10 min, maintaining an electrode separation of 1.3 cm (anodic deposition). In order to measure the coating thickness, FIB cross-sections were prepared with focused ion beam machining using 30 kV of bias.

### 2.4 Tribological Experiments

For the tribological experiments, a ball on disc tribometer (Nanotribometer from CSM Instruments) was used in a linear reciprocating sliding mode with a stroke length of  $600\text{ }\mu\text{m}$ . The normal load of 50 mN was applied using an alumina ball (purchased from Anton Paar GmbH) with a diameter of 6 mm, mounted on a cantilever with a stiffness of  $0.7624\text{ }\mu\text{N }\mu\text{m}^{-1}$  in normal and  $1.1447\text{ }\mu\text{N }\mu\text{m}^{-1}$  in tangential direction. Alumina is chosen to avoid any plastic deformation of the counter body. The surface roughness of the ball is not modified and used as delivered for all experiments. It is measured by WLI for ten different ball surfaces and a mean value of  $R_{\text{rms}} = 20 \pm 6\text{ nm}$  is determined. This is the best surface finish of commercially available alumina balls with a diameter of 6 mm we could purchase. The number of sliding cycles was set to 500 with a maximum sliding speed of 1 mm/s. The low load and low amount of sliding cycles are chosen in order to prevent severe wear and

thus not to change the surface roughness of the substrate material significantly during the experiment. Also, by applying low contact pressures, the particles are not hindered to freely move on the surfaces [31]. Temperature and relative humidity were kept constant at  $20 \pm 2$  °C and  $4 \pm 1$  %, respectively. A very low relative humidity is chosen in order to reduce lubrication effects based on a simple graphitic lubrication, which would need a higher relative humidity to be effective [67–69]. Three measurements were performed for each type of sample and the mean value of the coefficient of friction (COF) including standard deviation is plotted against the number of sliding cycles for each type of sample.

### 3 Results and discussion

After grinding and polishing the surfaces of the stainless steel platelets, they are analyzed using WLI as well as SEM. In **Fig. 1**, the different obtained surfaces are shown and the corresponding  $R_{rms}$  values including the standard deviations are given.

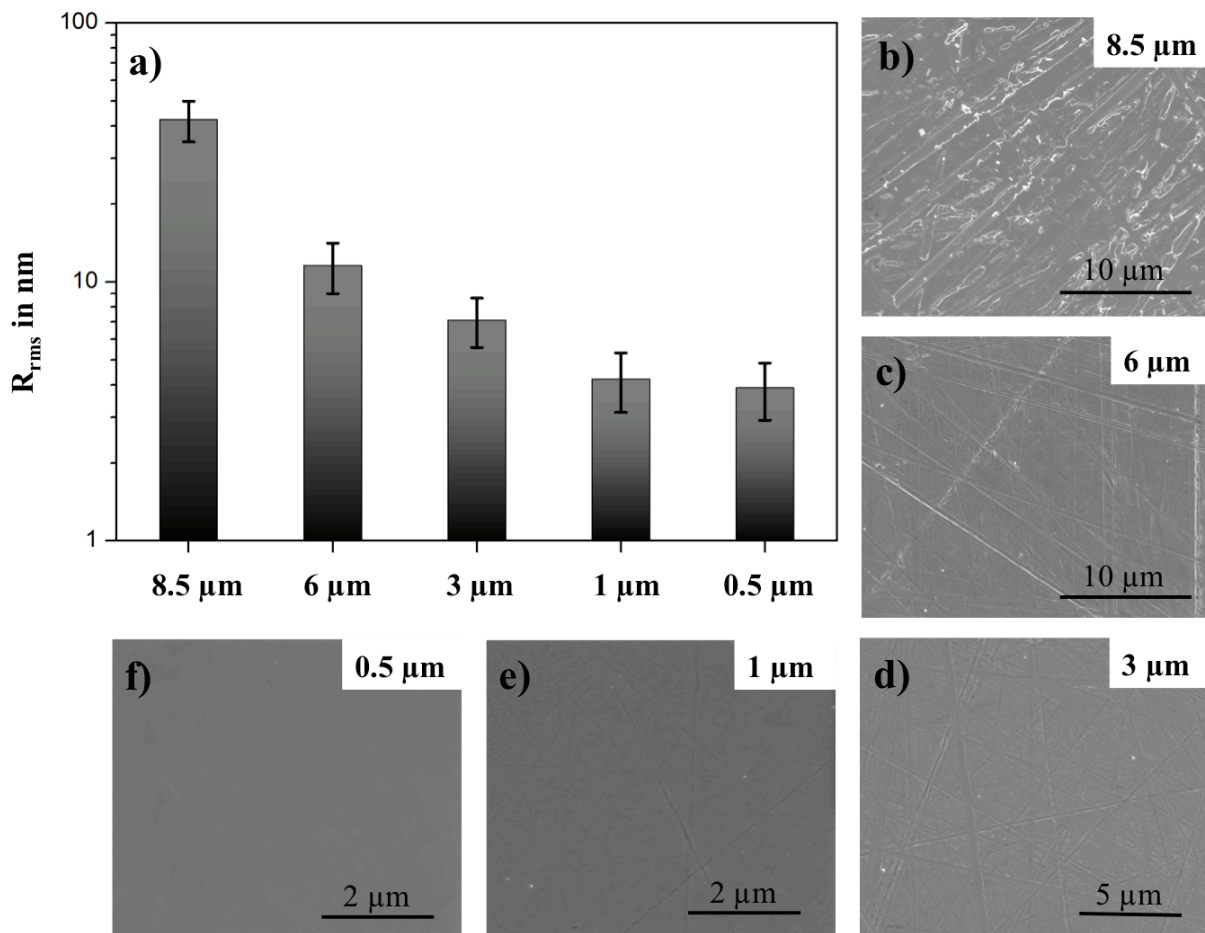


**Figure 1:** a)  $R_{rms}$  values of the prepared surfaces including the standard deviation before coating with CNT or OLC, respectively. The SEM micrographs correspond to b) 8.5  $\mu\text{m}$ , c) 6  $\mu\text{m}$ , d) 3  $\mu\text{m}$ , e) 1  $\mu\text{m}$  and f) 0.5  $\mu\text{m}$  surface finishing.

As expected, a clear decrease in the mean  $R_{rms}$  value is observed, from 42 nm in case of the preparation with sandpaper (8.5  $\mu\text{m}$ ) down to 3.9 nm for the oxide polishing suspension (0.5  $\mu\text{m}$ ). The SEM micrographs show large scratch-marks and even plastically deformed material in case of the sandpaper preparation (**Fig. 1a**). For the higher-grade surface finishing, these scratches are gradually removed until the marks reach the detection limit of the used techniques (in case of the 0.5  $\mu\text{m}$  polishing suspension) (**Fig. 1f**). During this surface preparation process, the samples were moved circularly over the rotating sandpaper or polishing cloth, keeping a

constant pressure. This is done to avoid the formation of anisotropic scratch-marks and results in the formation of randomly oriented scratch-marks on the steel surfaces.

Comparing these surfaces with the surface of the alumina ball ( $R_{\text{rms}} = 20 \pm 6 \text{ nm}$ ), the slightly larger standard deviation compared to the steel surfaces can be explained with 1-2  $\mu\text{m}$  sized, randomly appearing nicks in the alumina surface. However, the surface of each ball was studied by WLI before using it in the tribological experiment. Surfaces with marked nicks were consequently avoided.

The surfaces of the steel substrates are coated with CNT or OLC. The obtained coatings cover the surfaces homogeneously, as can be seen in **Fig. 2a, b**. However, there are clear differences between the two coatings. OLC form small agglomerates of a few 100 nm in diameter, that are stacked onto the metal surface. In case of CNT, a dense coating of intertwined CNT is observed, forming large agglomerates on the surface.

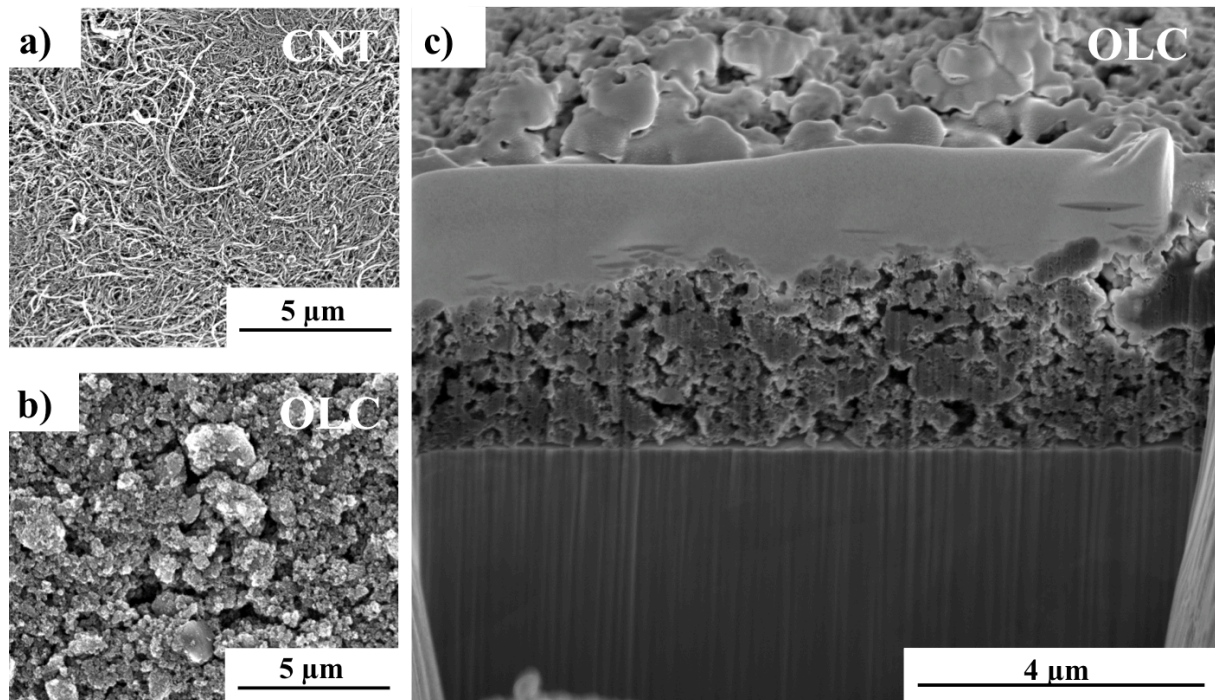


**Figure 2:** SEM micrographs of a) the CNT coating and b) the OLC coating on the steel surface with a 3  $\mu\text{m}$  finishing are shown. Also, the thickness of the OLC coating is demonstrated by a FIB cross-section in c).

In **Fig. 2c**, a FIB cross-section of the OLC coating on a 3  $\mu\text{m}$  polished steel surface is depicted. As exemplarily shown here, the thicknesses of the deposited coatings were measured. The achieved thicknesses are  $3 \pm 1 \mu\text{m}$  for the OLC coatings and  $3 \pm 2 \mu\text{m}$  for the CNT coatings. The CNT coatings show higher fluctuation in the coating thickness due to a higher tendency to form agglomerates, which has already been reported in previous studies [14, 65]. Furthermore, it is noticeable that the coating mainly consists of stacked small particle agglomerates, including a large quantity of pores in between the individual agglomerates (**Fig. 2c**). However, this is not considered as a debilitating factor for the tribological effects, as the coating will be compressed by the counterpart contacting the surface. Both types of coatings are not chemically bonded to the steel surface and show very low adhesion, being physisorption the only interdependency between coating and steel surface. This is done deliberately in order to allow a systematic study of the lubrication mechanism of the particles without

any chemical influence of the substrate by allowing the particles to move freely over the steel surface.

The different samples were then compared in terms of the temporal evolution of the COF for a maximum of 500 sliding cycles, which can be seen in **Fig. 3**.

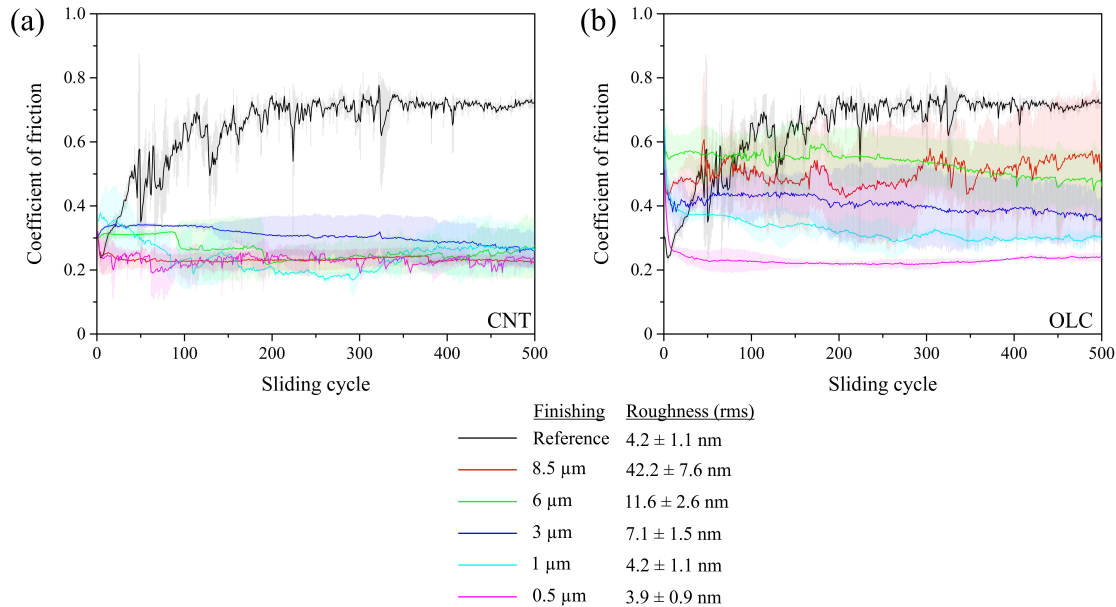


**Figure 3:** Temporal evolution of the dynamic COF as a function of the number of sliding cycles for a) CNT coated surfaces and b) OLC coated surfaces. The different colors correspond to different initial surfaces roughness as indicated below the graphs.

The reference COF corresponds to an uncoated steel surface with a finishing of 1  $\mu$ m ( $R_{\text{rms}} = 4.2 \pm 1.1$  nm). It is observed, that the COF increases during the first 250 cycles from 0.25 to 0.7, finally reaching steady state conditions. This behavior is well-known for pure metal surfaces and is extensively discussed in other works, for example in Blau et al. [70]. It can be explained with an increasing real contact area as a consequence of the combination of two effects; the wearing off of intrinsic asperities and an increment of the indentation depth of the ball into the substrate. The rather unstable evolution of the COF is related to the formation and disintegration of wear particles, which was also already examined in previous studies [14]. The obtained steady-state reference COF of 0.7 is in agreement with the value reported in the literature [71].

Regarding the CNT coated surfaces (**Fig. 3a**), a clear reduction of the COF can be observed. Furthermore, the impact of different surface roughness appears to be negligible as a COF of approximately 0.2 is sustained for all CNT coated surfaces after 500 sliding cycles. This is explained by the size and morphology of the CNTs. As the used CNTs present an outer diameter of 20-85 nm and a length of 5-15  $\mu$ m, they can effectively separate the two sliding surfaces with  $R_{\text{rms}}$  values between 3.9 and 42 nm. Although some of the surface scratches of the samples with higher roughness are larger than 85 nm in width, CNT could still be dragged out of these areas due to their high aspect ratio and their curved morphology with high flexibility. This allows CNTs to roll and/or to be degraded to nanocrystalline graphitic flakes and thus to lubricate the contact, as it was observed by Raman spectroscopy investigations in a previous study [14]. The slight variations in the frictional behavior of the different surfaces show no clear trend and provide a relatively large standard deviation. This is related to a varying thickness ( $3 \pm 2$   $\mu$ m) of the CNT coating in the different measuring areas. Considering the applied normal force (50 mN) and the coating thickness range (from a maximum of 5  $\mu$ m to a minimum of 1  $\mu$ m), partially entangled CNT have to be pulled by the alumina ball during the initial sliding

cycles, resulting in a varying tangential force until almost all the CNTs are shifted towards the end of the wear track. This will be further discussed in the wear track analysis.

Concerning the frictional behavior of the surfaces coated with OLC in **Fig. 3b**, a clear difference of the COF as a function of the pre-defined surface finishing is noticeable. For the COF evolution of the 8.5  $\mu\text{m}$  ( $R_{\text{rms}} = 42 \pm 7.5 \text{ nm}$ ) and 6  $\mu\text{m}$  ( $R_{\text{rms}} = 11.5 \pm 2.5 \text{ nm}$ ) samples, only a marginal frictional reduction can be observed after the first 100 sliding cycles until the end of the measurement. As the roughness of these surfaces are evidently larger than the diameter of the OLC particles (4 – 10 nm), it seems reasonable to state that the OLCs are trapped within the surface scratch marks and are being removed from the direct contact zone, as already reported by Hirata et al. [28]. Still, some of the particles remain in direct tribological contact, contributing to the slight reduction of the mean value of the COF. However, the high fluctuation of the COF in case of the 8.5  $\mu\text{m}$  surface finishing is comparable with the behavior of the reference. Therefore, it becomes clear that the acting tribo-mechanisms of both samples are similar and most likely dominated by the direct contact of the alumina ball with the steel surface.

By analyzing the higher grade surface finishes (3  $\mu\text{m}$  ( $R_{\text{rms}} = 7.1 \pm 1.5 \text{ nm}$ ), 1  $\mu\text{m}$  ( $R_{\text{rms}} = 4.2 \pm 1 \text{ nm}$ ) and 0.5  $\mu\text{m}$  ( $R_{\text{rms}} = 3.9 \pm 0.9 \text{ nm}$ )), the COF is gradually decreasing and the standard deviations are clearly reduced. Considering that the  $R_{\text{rms}}$  values (7.1 nm – 3.9 nm) are now in the range of the particle diameter, a separation of the two sliding surfaces by OLC is conceivable. This leads to a stabilization of the COF evolution and thus explains the reduced standard deviation. As discussed in the introduction, the OLC morphology, low amount of dangling bonds and their high strength make it reasonable to assume that they are acting as rolling elements, efficiently reducing the friction coefficient. However, the COF of the system is not reaching values below 0.2, as observed by Hirata et al. [28]. This might be a consequence of the counterpart roughness ( $R_{\text{rms}}$  of 20 nm), being able to trap OLC particles within the surface asperities. Nonetheless, an effect on the COF by surface roughness variation of the substrate material is clearly noticeable.

In order to achieve a better understanding of the acting tribo-mechanisms, the wear-tracks have to be analyzed in more detail. **Fig 4** shows two SEM micrographs of single MWCNT on the steel surface (3  $\mu\text{m}$  surface finishing) after the tribological experiment with the given sliding direction (S.D.).

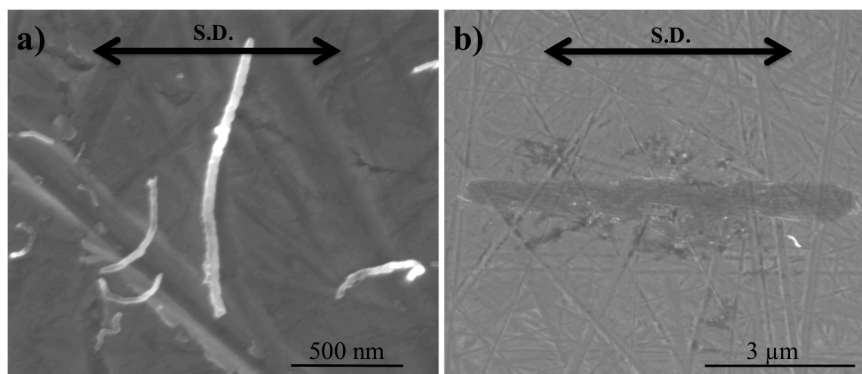


**Figure 4:** SEM micrographs of a) shortened MWCNT, oriented perpendicular to the sliding direction (S.D.) on a 3  $\mu\text{m}$  surface and b) One single damaged, delaminated MWCNT, oriented parallel to the sliding direction (S.D.) on a 3  $\mu\text{m}$  surface.

The SEM micrographs exemplify the dimensions of the scratch-marks of a 3  $\mu\text{m}$  sample surface compared to the used MWCNT. These micrographs support the assumption, that MWCNT cannot be trapped within the roughness of the prepared surfaces. Considering the structural integrity of the particles, the MWCNT

oriented perpendicular to the sliding direction seem to be unmodified and only slightly shorter than the initial length of 5-15  $\mu\text{m}$  (**Fig 4a**). This fact supports the assumption of MWCNT are able to roll on the surface. In contrast to that, the MWCNT which is aligned in parallel to the sliding direction, appears to be fully degraded and delaminated (**Fig 4b**). This observation is consistent with Raman spectroscopy studies of previous works, describing the transition of MWCNT towards nanocrystalline graphite in a tribological contact [14]. The demonstrated situations represent the extreme possible cases and, as the MWCNT coating consists of randomly oriented particles, the lubrication mechanism almost certainly consists of a mixture of both cases.

In **Fig. 5**, the wear tracks of a) the 3  $\mu\text{m}$  surface coated with CNT and b) the 3  $\mu\text{m}$  surface coated with OLC are shown. In both cases, besides the shifted coating towards the end of the wear tracks, no sign of severe wear of the substrate steel material is observed after 500 sliding cycles.

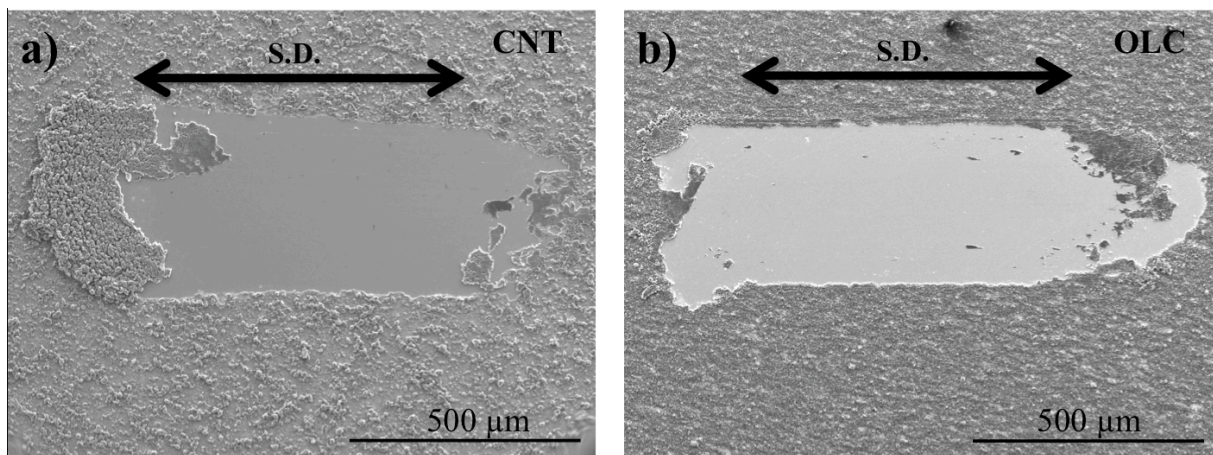


**Figure 5:** SEM micrographs of the wear track after the tribological experiment of the 3  $\mu\text{m}$  steel substrate coated with a) CNT and b) OLC. In both cases, no severe wear of the substrate material is observed. The sliding direction (S.D.) is indicated with an arrow.

This fact also supports the assumption, that both surfaces are effectively separated by the particles when their diameter is in the range of the surface roughness. Thus, it can be concluded that the tribological contact is dominated by the separation of the two surfaces by the carbon nanoparticles and not by a direct interaction of the substrate steel with the alumina ball. This observation correlates well with the reduction of the COF in **Fig. 3** as energy losses due to plastic deformation or adhesion of the potentially contacting surfaces could be avoided. Furthermore, the shift of the carbon nanoparticle (CNP) coatings towards the end of the wear track takes place within the initial sliding cycles and therefore can be correlated with the initially high COF values. Considering the very low normal load of 50 mN, this is reasonable, as a slightly higher tangential force is needed in order to shift the agglomerated particle coatings towards the ends of the wear track, resulting in a higher COF. Particularly for the CNT coated surfaces, this effect is more pronounced as the CNT form an entangled network on the substrate surface. Thus, mechanically entangled CNT are piled up at the left hand side of the wear track. Although this shifting of the coating happens within the initial sliding cycles, the lubrication effect is present for the entire experiment, showing that only few CNPs need to be in direct tribological contact for an efficient lubrication as most of them are dragged out of the direct contact area.

**Fig. 6** presents the wear tracks of the 8.5  $\mu\text{m}$ -finished surfaces coated with CNT or OLC, respectively. It is noticeable, that the direct tribological contact zone in the middle of the SEM micrographs is by far less wide than the area of the removed coating. This can be explained by two facts. First, if the alumina ball applies pressure to the surface, only the center and its vicinity is in direct contact to the substrate material. The flanks of

the alumina ball are only in contact with the coating, which is shifted with the moving ball. Second, as the particles are agglomerated and entangled, coated areas that were not in direct contact to the alumina ball might be pulled by moving neighboring particles. Overall, this leads to the observed broad removal of the coating around the direct tribological contact zone. Furthermore, the wear-track of the CNT coating (**Fig. 6a**) does not show any appearance of severe wear of the substrate material with the initially produced scratch-marks of the surface preparation still being identifiable (**Fig. 6c**). However, the formation of a grey layer and filled scratch-marks indicate the possibility of storing degraded MWCNT. Nevertheless, the lubrication effect of this system is still active, as can be seen in **Fig. 3a**. In contrast to that, **Fig 6b** and **d** clearly exhibit signs of severe wear as anisotropic scratch-marks parallel to the sliding direction are formed. This indicates, that OLCs lose their ability to separate both surfaces, which is in agreement with the evolution of the COF. Furthermore, OLC particles are trapped within the as-prepared surface scratch-marks, therefore not participating in the direct tribological contact to any further extent (**Fig. 6d**). For the 6  $\mu\text{m}$  surfaces, similar observations were made.

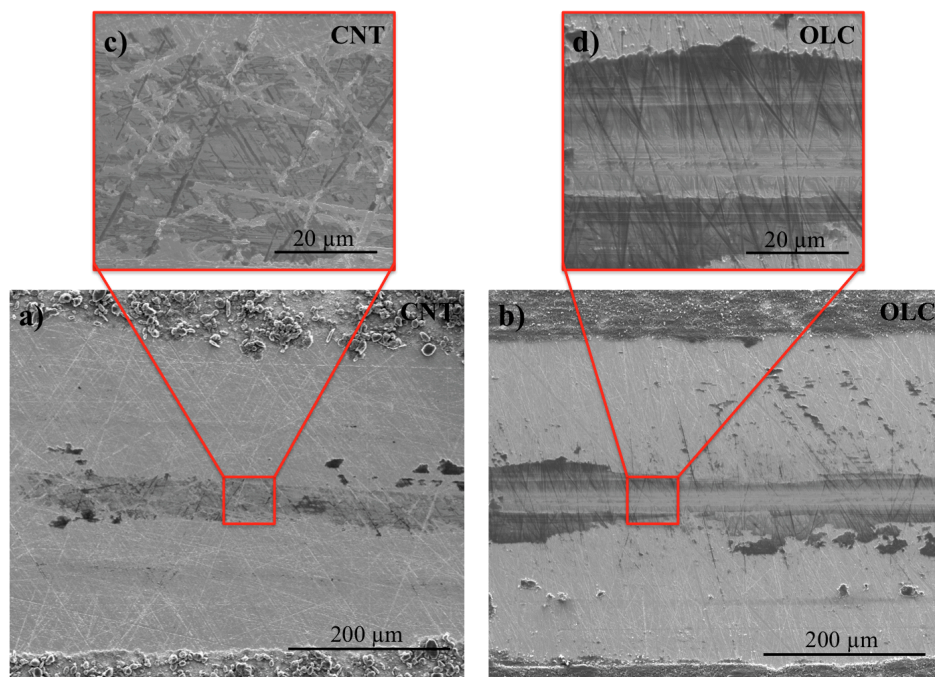


**Figure 6:** SEM micrographs of the wear tracks after the tribological experiment on the 8.5  $\mu\text{m}$  surfaces coated with a) MWCNT and b) OLC. Higher magnification SEM micrographs show the scratch-marks in more detail and are depicted in c) for CNT and d) for OLC. Severe wear is only observed for the OLC coated surface.

Looking in detail at the wear-tracks of the 3  $\mu\text{m}$ -finished surfaces (**Fig 7**), differences between both coatings can be observed again. In case of the CNT-coated sample, the surface is in pristine condition after the tribological experiment (500 sliding cycles) and no particle trapping is noticed, even with higher magnification. For the OLC coating, although no severe wear is observed, particles are partially stored in the scratch-marks of the surface. Thus, the contacting surfaces of ball and substrate can still be separated, but the possible rolling mechanism of the OLC appears to be strongly hindered, as analyzed in the COF measurement in **Fig. 3b**.

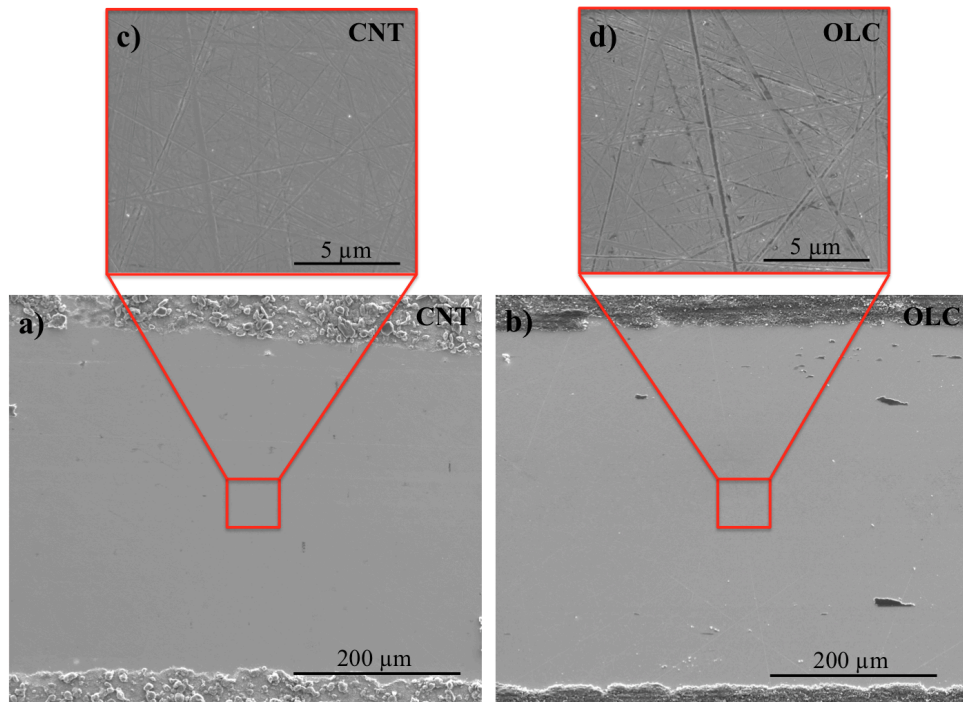


**Figure 7:** SEM micrographs of the wear tracks after the tribological experiment on the 3  $\mu\text{m}$  surfaces coated with a) MWCNT and b) OLC. Higher magnification SEM micrographs show the scratch-marks in more detail and are depicted in c) for CNT and d) for OLC.

In **Fig. 8**, a single scratch mark of the OLC wear track in **Fig. 7 b and d** is shown under high magnification, marked with red lines. OLC particles are observed between the red lines, which are stored in the scratch mark thus severely restricting their ability to freely move or roll on the surface.

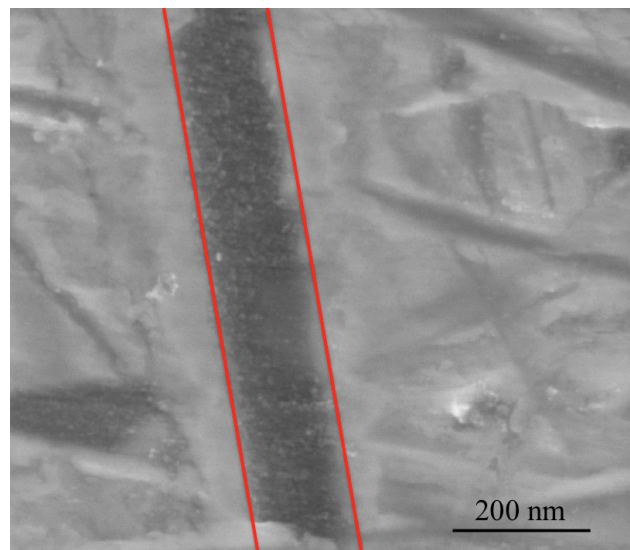


**Figure 8:** High magnification SEM micrograph of a scratch mark (marked in red) within the wear track of the 3  $\mu\text{m}$  surface coated with OLC after the experiment. It can be seen, that the scratch mark is filled with trapped OLC particles that cannot efficiently roll on the surface therefore providing no pronounced lubrication effect.

For the 1  $\mu\text{m}$ - and 0.5  $\mu\text{m}$ -finished surfaces, no particle trapping is found, neither in case of CNT nor in the OLC coatings. This explains the decreasing COF in case of the OLC coatings, as less surface scratch-marks can interfere with the potential rolling mechanism of the particles.

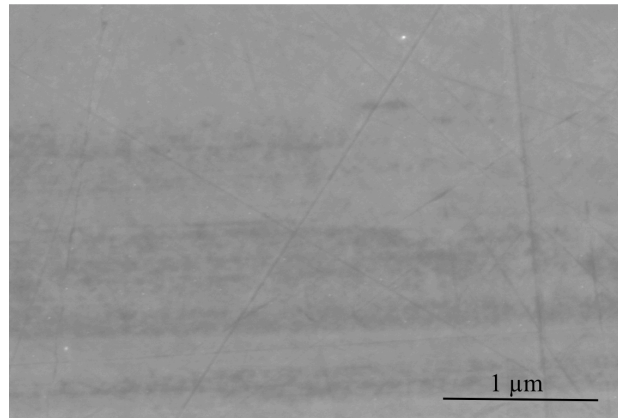


**Figure 9:** High magnification SEM micrograph of the wear track after the tribological experiment on the 1 μm surface coated with MWCNT. The surface is representative for the OLC coating as well.

However, by observing at very high magnification in the SEM (**Fig 8**), grey-shaded areas are detected in the wear-tracks for both coatings. These areas might result from the degradation of the carbon particles in the direct tribological contact, thus forming nanocrystalline graphitic layers as already reported by Reinert et al. [14]. Thus, the lubrication mechanism of both types of particles is traced back to a mixture between a rolling motion on the surfaces and particle degradation, including the formation of nanocrystalline graphitic layers. Summarizing, this investigation highlights that choosing the suitable surface finish for a tribological application is crucial for achieving beneficial tribological effects of CNP lubricated surfaces.

#### 4 Conclusions

In the present study, a systematic evaluation of the influence of surface roughness on the lubrication activity of MWCNT and OLC has been carried out. It was observed that the friction coefficient of the steel surfaces (against alumina counterbodies) can be decreased considerably from 0.7 to 0.2 after applying an electrophoretically deposited OLC or MWCNT coating. The degree of frictional reduction in case of OLC is increasing with decreasing surface roughness. For a roughness higher than the diameter of the OLC particles (4-10 nm), only marginal lubrication is observed. This is explained by the particles being trapped within the initially induced surface scratch-marks, therefore not being able to separate the contacting surfaces. When the surface roughness is in the range of the OLC particle diameter or below, efficient lubrication is observed. For MWCNT, no dependence of the lubrication activity on the surface roughness is observed. This is explained by their larger diameter (20-85 nm) and high aspect ratio (length of 5-15 μm), allowing them to be dragged inside of the direct tribological contact region. The lubrication mechanism of both types of particles is traced back to a mixture between a rolling motion on the surfaces and particle degradation, including the formation of nanocrystalline graphitic layers. However, it is assumed, that the lubrication effect for both particles would be even more pronounced in case of a smoother surface of the ball ( $R_{\text{rms}} = 20 \pm 6$  nm), as it might hinder the particles in their rolling mechanism. The aforementioned results emphasize that, in order to achieve beneficial tribological effects of carbon nanoparticle lubricated surfaces, the choice of a suitable surface finish for a tribological application is of utmost importance.

## References

1. Holmberg, K., Andersson, P., Erdemir, A.: Global energy consumption due to friction in passenger cars. *Tribol. Int.* 47, 221–234 (2012). doi:10.1016/j.triboint.2011.11.022
2. Donnet, C., Erdemir, A.: Solid Lubricant Coatings: Recent Developments and Future Trends. *Tribol. Lett.* 17, 389–397 (2004)
3. Aouadi, S.M., Gao, H., Martine, A., Scharf, T.W., Muratore, C.: Lubricious oxide coatings for extreme temperature applications: A review. *Surf. Coatings Technol.* 257, 266–277 (2014)
4. Li, Y., Li, B.X., Zou, W.J.: The Relationship between Nanocrystalline Structure and Frictional Properties of Nanodiamond/Ni Composite Coatings by Brush Plating. *Appl. Mech. Mater.* 80-81, 683–687 (2011). doi:10.4028/www.scientific.net/AMM.80-81.683
5. Hirata, A., Yoshioka, N.: Sliding friction properties of carbon nanotube coatings deposited by microwave plasma chemical vapor deposition. *Tribol. Int.* 37, 893–898 (2004). doi:10.1016/j.triboint.2004.07.005
6. Miyoshi, K., Jr., K.W.S., Wal, R.L. Vander, Andrews, R., Sayir, A.: Solid lubrication by multiwalled carbon nanotubes in air and in vacuum. *Tribol. Lett.* 19, 191–201 (2005). doi:10.1007/s11249-005-6146-4
7. Reinert, L., Suárez, S., Rosenkranz, A.: Tribo-Mechanisms of Carbon Nanotubes: Friction and Wear Behavior of CNT-Reinforced Nickel Matrix Composites and CNT-Coated Bulk Nickel. *Lubricants.* 4, 11 (2016). doi:10.3390/lubricants4020011
8. Gogotsi, Y., Presser, V.: *Carbon Nanomaterials.* (2014). CRC Press. ISBN 9781138076815
9. Bakshi, S.R., Lahiri, D., Agarwal, A.: Carbon nanotube reinforced metal matrix composites - a review. *Int. Mater. Rev.* 55, 41–64 (2010). doi:10.1179/095066009X12572530170543
10. Mochalin, V.N., Shenderova, O., Ho, D., Gogotsi, Y.: The properties and applications of nanodiamonds. *Nat. Nanotechnol.* 7, 11–23 (2012). doi:10.1038/nnano.2011.209
11. Iijima, S.: Helical microtubules of graphitic carbon. *Nature.* 354, 56–58 (1991)
12. Cebik, J., McDonough, J.K., Peerally, F., Medrano, R., Neitzel, I., Gogotsi, Y., Osswald, S.: Raman spectroscopy study of the nanodiamond-to-carbon onion transformation. *Nanotechnology.* 24, 1–10 (2013). doi:10.1088/0957-4484/24/20/205703
13. Zeiger, M., Jäckel, N., Aslan, M., Weingarh, D., Presser, V.: Understanding structure and porosity of nanodiamond-derived carbon onions. *Carbon* 84, 584–598 (2015). doi:10.1016/j.carbon.2014.12.050
14. Reinert, L., Lasserre, F., Gachot, C., Grützmacher, P., MacLucas, T., Souza, N., Mücklich, F., Suarez, S.: Long-lasting solid lubrication by CNT-coated patterned surfaces. *Sci. Rep.* 7 (2017). doi:10.1038/srep42873
15. Hu, J.J., Jo, S.H., Ren, Z.F., Voevodin, A., Zabinski, J.S.: Tribological behavior and graphitization of carbon nanotubes grown on 440C stainless steel. *Tribol. Lett.* 19, 119–125 (2005). doi:10.1007/s11249-005-5091-6
16. Dickrell, P.L., Pal, S.K., Bourne, G.R., Muratore, C., Voevodin, a. a., Ajayan, P.M., Schadler, L.S., Sawyer, W.G.: Tunable friction behavior of oriented carbon nanotube films. *Tribol. Lett.* 24, 85–90 (2006). doi:10.1007/s11249-006-9162-0
17. Zhang, X., Luster, B., Church, A., Muratore, C., Voevodin, A. a, Kohli, P., Aouadi, S., Talapatra, S.: Carbon nanotube-MoS<sub>2</sub> composites as solid lubricants. *ACS Appl. Mater. Interfaces.* 1, 735–9 (2009).

doi:10.1021/am800240e

18. Arai, S., Fujimori, A., Murai, M., Endo, M.: Excellent solid lubrication of electrodeposited nickel-multiwalled carbon nanotube composite films. *Mater. Lett.* 62, 3545–3548 (2008).  
doi:10.1016/j.matlet.2008.03.047
19. Chen, W.X., Tu, J.P., Wang, L.Y., Gan, H.Y., Xu, Z.D., Zhang, X.B.: Tribological application of carbon nanotubes in a metal-based composite coating and composites. *Carbon* 41, 215–222 (2003)
20. Kim, K.T., Cha, S. Il, Hong, S.H.: Hardness and wear resistance of carbon nanotube reinforced Cu matrix nanocomposites. *Mater. Sci. Eng. A.* 449–451, 46–50 (2007). doi:10.1016/j.msea.2006.02.310
21. Scharf, T.W., Neira, A., Hwang, J.Y., Tiley, J., Banerjee, R.: Self-lubricating carbon nanotube reinforced nickel matrix composites. *J. Appl. Phys.* 106, 013508 (2009). doi:10.1063/1.3158360
22. Chen, C.S., Chen, X.H., Xu, L.S., Yang, Z., Li, W.H.: Modification of multi-walled carbon nanotubes with fatty acid and their tribological properties as lubricant additive. *Carbon* 43, 1660–1666 (2005).  
doi:10.1016/j.carbon.2005.01.044
23. Peng, Y., Hu, Y., Wang, H.: Tribological behaviors of surfactant-functionalized carbon nanotubes as lubricant additive in water. *Tribol. Lett.* 25, 247–253 (2006). doi:10.1007/s11249-006-9176-7
24. Lu, H.F., Fei, B., Xin, J.H., Wang, R.H., Li, L., Guan, W.C.: Synthesis and lubricating performance of a carbon nanotube seeded miniemulsion. *Carbon* 45, 936–942 (2007). doi:10.1016/j.carbon.2007.01.001
25. Dickrell, P.L., Sinnott, S.B., Hahn, D.W., Ravikiran, N.R., Schadler, L.S., Ajayan, P.M., Sawyer, W.G.: Frictional anisotropy of oriented carbon nanotube surfaces. *Tribol. Lett.* 18, 59–62 (2005).  
doi:10.1007/s11249-004-1752-0
26. Ni, B., Sinnott, S.B.: Tribological properties of carbon nanotube bundles predicted from atomistic simulations. *Surf. Sci.* 487, 87–96 (2001). doi:10.1016/S0039-6028(01)01073-1
27. Martin, J.M., Ohmae, N.: *Nanolubricants*. (2008). John Wiley & Sons, ISBN: 978-0-470-06552-5
28. Hirata, A., Igarashi, M., Kaito, T.: Study on solid lubricant properties of carbon onions produced by heat treatment of diamond clusters or particles. *Tribol. Int.* 37, 899–905 (2004).  
doi:10.1016/j.triboint.2004.07.006
29. Park, S., Srivastava, D., Cho, K.: Generalized Chemical Reactivity of Curved Surfaces: Carbon Nanotubes. *Nano Lett.* 3, 1273–1277 (2003). doi:10.1021/nl0342747
30. Street, K.W., Marchetti, M., Wal, R.L. Vander, Tomasek, A.J.: Evaluation of the tribological behavior of nano-onions in Krytox 143AB. *Tribol. Lett.* 16, 143–149 (2004)
31. Bucholz, E.W., Phillpot, S.R., Sinnott, S.B.: Molecular dynamics investigation of the lubrication mechanism of carbon nano-onions. *Comput. Mater. Sci.* 54, 91–96 (2012).  
doi:10.1016/j.commatsci.2011.09.036
32. Menezes, P.L., Kishore, Kailas, S. V.: Effect of surface roughness parameters and surface texture on friction and transfer layer formation in tin-steel tribo-system. *J. Mater. Process. Technol.* 208, 372–382 (2008). doi:10.1016/j.jmatprotec.2008.01.003
33. Persson, B.N.J., Albohr, O., Tartaglino, U., Volokitin, A.I., Tosatti, E.: On the nature of surface roughness with application to contact mechanics, sealing, rubber friction and adhesion. *J. Phys. Condens. Matter.* 17, (2005). doi:10.1088/0953-8984/17/1/R01
34. Sahin, M., Çetinarslan, C.S., Akata, H.E.: Effect of surface roughness on friction coefficients during upsetting processes for different materials. *Mater. Des.* 28, 633–640 (2007).

doi:10.1016/j.matdes.2005.07.019

35. Svahn, F., Kassman-Rudolphi, Å., Wallén, E.: The influence of surface roughness on friction and wear of machine element coatings. *Wear*. 254, 1092–1098 (2003). doi:10.1016/S0043-1648(03)00341-7
36. Komvopoulos, K.: Adhesion and friction forces in microelectromechanical systems: mechanisms, measurement, surface modification techniques, and adhesion theory. *J. Adhes. Sci. Technol.* 17, 477–517 (2003). doi:10.1163/15685610360554384
37. Bowden, F.P. Tabor, D.: Mechanism of metallic friction. *Nature*. 3798, 197–199 (1942). doi:10.1038/150197a0
38. Czichos, H., Habig, K.: *Tribologie-Handbuch*. (2010). Vieweg + Teubner. ISBN 978-3-8348-0017-6
39. Hirano, M., Shinjo, K., Kaneko, R., Murata, Y.: Anisotropy of frictional forces in muscovite mica. *Phys. Rev. Lett.* 67, 2642–2646 (1991)
40. Dienwiebel, M., Verhoeven, G., Pradeep, N., Frenken, J., Heimberg, J., Zandbergen, H.: Superlubricity of Graphite. *Phys. Rev. Lett.* 92, 126101 (2004). doi:10.1103/PhysRevLett.92.126101
41. Tomlinson, G.A.: A molecular theory of friction. *London, Edinburgh, Dublin Philos. Mag. J. Sci.* 7, 905–939 (1929). doi:10.1080/14786440608564819
42. Weiss, M., Elmer, F.: Dry friction in the Frenkel-Kontorova-Tomlinson model: Static properties. *Phys. Rev. B. Condens. Matter.* 53, 7539–7549 (1996)
43. Etsion, I.: State of the Art in Laser Surface Texturing. *J. Tribol. Trans. ASME.* 127, 248 (2005). doi:10.1115/1.1828070
44. Rapoport, L., Moshkovich, A., Perfilyev, V., Gedanken, A., Koltypin, Y., Sominski, E., Halperin, G., Etsion, I.: Wear life and adhesion of solid lubricant films on laser-textured steel surfaces. *Wear*. 267, 1203–1207 (2009). doi:10.1016/j.wear.2009.01.053
45. Gachot, C., Rosenkranz, A., Reinert, L., Ramos-Moore, E., Souza, N., Müser, M.H., Mücklich, F.: Dry Friction Between Laser-Patterned Surfaces: Role of Alignment, Structural Wavelength and Surface Chemistry. *Tribol. Lett.* 9, 193–202 (2013). doi:10.1007/s11249-012-0057-y
46. Rosenkranz, A., Reinert, L., Gachot, C., Mücklich, F.: Alignment and wear debris effects between laser-patterned steel surfaces under dry sliding conditions. *Wear*. 318, 49–61 (2014). doi:10.1016/j.wear.2014.06.016
47. Sondhauf, J., Fuchs, H., Schirmeisen, A.: Frictional Properties of a Mesoscopic Contact with Engineered Surface Roughness. *Tribol. Lett.* 42, 319–324 (2011)
48. Persson, B.N.J.: Contact mechanics for randomly rough surfaces. *Surf. Sci. Rep.* 61, 201–227 (2006). doi:10.1016/j.surfrep.2006.04.001
49. Greenwood, J., Williamson, J.: Contact of nominally flat surfaces. *R. Soc. Publ.* 295, 300–319 (1966)
50. Jackson, R.L., Green, I.: A statistical model of elasto-plastic asperity contact between rough surfaces. *Tribol. Int.* 39, 906–914 (2006). doi:10.1016/j.triboint.2005.09.001
51. Akbulut, M.: Nanoparticle-Based Lubrication Systems. *J. Powder Metall. Min.* 1, 377–411 (2012). doi:10.1002/9781118483961.ch17
52. Wu, Y.Y., Tsui, W.C., Liu, T.C.: Experimental analysis of tribological properties of lubricating oils with nanoparticle additives. *Wear*. 262, 819–825 (2007). doi:10.1016/j.wear.2006.08.021
53. Ivanov, M.G., Ivanov, D.M., Pavlyshko, S. V., Petrov, I., Vargas, A., McGuire, G., Shenderova, O.: Nanodiamond-Based Nanolubricants. Fullerenes, Nanotub. Carbon Nanostructures. 20, 606–610 (2012).

doi:10.1080/1536383X.2012.657010

54. Joly-Pottuz, L., Vacher, B., Ohmae, N., Martin, J.M., Epicier, T.: Anti-wear and Friction Reducing Mechanisms of Carbon Nano-onions as Lubricant Additives. *Tribol. Lett.* 30, 69–80 (2008). doi:10.1007/s11249-008-9316-3
55. Khalilpourazary, S., Meshkat, S.S.: Investigation of the effects of alumina nanoparticles on spur gear surface roughness and hob tool wear in hobbing process. *Int. J. Adv. Manuf. Technol.* 71, 1599–1610 (2014). doi:10.1007/s00170-013-5591-8
56. Rahmati, B., Sarhan, A.A.D., Sayuti, M.: Investigating the optimum molybdenum disulfide (MoS<sub>2</sub>) nanolubrication parameters in CNC milling of AL6061-T6 alloy. *Int. J. Adv. Manuf. Technol.* 70, 1143–1155 (2014). doi:10.1007/s00170-013-5334-x
57. Hwang, Y., Lee, C., Choi, Y., Cheong, S., Kim, D., Lee, K., Lee, J., Kim, S.H.: Effect of the size and morphology of particles dispersed in nano-oil on friction performance between rotating discs. *J. Mech. Sci. Technol.* 25, 2853–2857 (2011). doi:10.1007/s12206-011-0724-1
58. Kogovšek, J., Remškar, M., Mrzel, A., Kalin, M.: Influence of surface roughness and running-in on the lubrication of steel surfaces with oil containing MoS<sub>2</sub> nanotubes in all lubrication regimes. *Tribol. Int.* 61, 40–47 (2013). doi:10.1016/j.triboint.2012.12.003
59. Tevet, O., Von-Huth, P., Popovitz-Biro, R., Rosentsveig, R., Wagner, H.D., Tenne, R.: Friction mechanism of individual multilayered nanoparticles. *Proc. Natl. Acad. Sci.* 108, 19901–19906 (2011). doi:10.1073/pnas.1106553108
60. Majumder, M., Rendall, C., Li, M., Behabtu, N., Eukel, J.A., Hauge, R.H., Schmidt, H.K., Pasquali, M.: Insights into the physics of spray coating of SWNT films. *Chem. Eng. Sci.* 65, 2000–2008 (2010). doi:10.1016/j.ces.2009.11.042
61. Mirri, F., Ma, A.W.K., Hsu, T.T., Behabtu, N., Eichmann, S.L., Young, C.C., Tsentlovich, D.E., Pasquali, M.: High-Performance Carbon Nanotube Transparent Conductive Films by Scalable Dip Coating. 9737–9744 (2012)
62. De Nicola, F., Castrucci, P., Scarselli, M., Nanni, F., Cacciotti, I., De Crescenzi, M.: Super-hydrophobic multi-walled carbon nanotube coatings for stainless steel. *Nanotechnology.* 26, 145701 (2015). doi:10.1088/0957-4484/26/14/145701
63. Boccaccini, A.R., Cho, J., Roether, J. a., Thomas, B.J.C., Jane Minay, E., Shaffer, M.S.P.: Electrophoretic deposition of carbon nanotubes. *Carbon* 44, 3149–3160 (2006). doi:10.1016/j.carbon.2006.06.021
64. Besra, L., Liu, M.: A review on fundamentals and applications of electrophoretic deposition (EPD). *Prog. Mater. Sci.* 52, 1–61 (2007). doi:10.1016/j.pmatsci.2006.07.001
65. Reinert, L., Zeiger, M., Suarez, S., Presser, V., Mücklich, F.: Dispersion analysis of carbon nanotubes, carbon onions, and nanodiamonds for their application as reinforcement phase in nickel metal matrix composites. *RSC Adv.* 5, 95149–95159 (2015). doi:10.1039/C5RA14310A
66. De Riccardis, M.F., Carbone, D., Rizzo, a: A novel method for preparing and characterizing alcoholic EPD suspensions. *J. Colloid Interface Sci.* 307, 109–115 (2007). doi:10.1016/j.jcis.2006.10.037
67. Yen, B.K., Ishihara, T.: Effect of humidity on friction and wear of Al-Si eutectic alloy and Al-Si alloy-graphite composites. *Wear.* 198, 169–175 (1996)
68. Savage, R.H.: Graphite Lubrication. *J. Appl. Phys.* 19, 1 (1948). doi:10.1063/1.1697867

69. Berman, D., Erdemir, A., Sumant, A. V.: Graphene: A new emerging lubricant. *Mater. Today*. 17, 31–42 (2014). doi:10.1016/j.mattod.2013.12.003
70. Blau, P.J.: On the nature of running-in. *Tribol. Int.* 38, 1007–1012 (2005). doi:10.1016/j.triboint.2005.07.020
71. Dogan, H., Findik, F., Morgul, O.: Friction and wear behaviour of implanted AISI 316L SS and comparison with a substrate. *Mater. Des.* 23, 605–610 (2002). doi:http://dx.doi.org/10.1016/S0261-3069(02)00066-3